Passive and Active Hybrid Integrated EMI Filters

J. Biela, A. Wirthmueller, R. Waespe,
M. L. Heldwein, J. W. Kolar
Power Electronic Systems Laboratory
Swiss Federal Institute of Technology
Zurich, Switzerland
Email: biela@lem.ee.ethz.ch

E. Waffenschmidt
Philips Research Laboratories
52066 Aachen, Germany
Email: eberhard.waffenschmidt@philips.com

***Abstract*— Two new planar integrated EMI filter structures which reduce the filter volume and which are based on standard PCB process technology are presented in this paper.**

First, a passive integrated EMI filter is presented, which results in a volume reduction of 25% compared to the discrete solution. However, this filter requires a planar ferrite core for the CM inductor.

In order to eliminate the ferrite core and reduce the filter volume further (-40% vs. discrete filter) a passive integrated structure is combined with an active EMI filtering circuit.

The transfer function, the volume and the losses of the discrete and the two integrated filters, which are designed for a 600W PFC converter, are compared.

I. Introduction

The pursuit of obtaining higher power density AC/DC and DC/DC converters leads to increasing switching frequencies in order to reduce the size of the energy storage elements. These energy storage elements usually influence the overall size of a converter significantly. This has resulted in the development of electromagnetically integrated structures [1], which combine several functions in one passive component.

Due to increasing switching frequencies, conducted emissions from 150kHz to 30MHz have increased. Thus, the EMI filter has become also a significant part of the converter in terms of size and cost. For this reason some electromagnetically integrated EMI filter structures [2] & [4] and also active EMI filters [5] & [6] have been proposed.

In this paper two new planar EMI filter structures are presented which allow a significant reduction of the filter volume. These structures are integrated in a PCB, which could be manufactured using a cost-saving standard PCB manufacturing process.

With the first filter structure all inductor windings and all capacitors except for a large differential mode capacitor are integrated in the PCB. The DM capacitor is realised by a parallel connection of X2 SMD-X7R capacitors. For the large inductance value of the CM choke a planar ferrite core is needed. Although, the overall filter has a very low profile (height < 9.5 mm) and a low volume ($\approx$25% volume reduction in comparison to a discrete solution). This filter is called Passive Hybrid Integrated EMI Filter due to the combination of integrated and discrete passive components.

In a second step the passive integrated structure is combined with an analog amplifier (active EMI-filter). With the amplifier stage the required inductance and capacitance values of the components decrease significantly, so that no additional ferrite core is needed. The components of the active filter are mounted on top of the PCB, in where the passive filter is integrated. This new approach results in a very compact construction ($\approx$ 40% volume reduction in comparison to a discrete solution) and is called Active Hybrid Integrated EMI Filter.

Table I: Specification of PFC-converter

Parameter	Value
Output Power	600W
Output Voltage	410V
Switching Frequency	250kHz
Input Voltage (incl. tolerances)	110V - 230V (93V - 264V)
Input Current (incl. tolerances)	2.6A - 5.5A (2.3A - 6.5A)

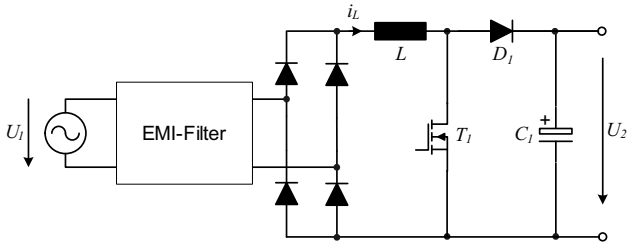

Figure 1: Circuit Diagram of a 600W PFC

The two proposed filter structures are designed for a 600W PFC-converter intended for IT applications (cf. fig. 1) with the specification given in table I. In **section II** of the paper the discrete EMI-filter for the PFC converter is described for comparing the new structures with a conventional filter. The structure of the passive hybrid integrated EMI filter, which is designed and optimised using FEM simulations, is presented in **section III**. Thereafter, the mode of operation and the design of the active hybrid integrated EMI filter is explained in **section IV**. The measured transfer functions of all three filters together with the losses/efficiency and the volume are compared in **section V**. Finally, a conclusion and topics of future research are given in **section VI**.

II. Discrete EMI-filter

The discrete EMI filter is designed according to the procedure described in [10] and [11], which is summarised shortly in the following. First, the DM and CM conducted emissions of the PFC converter are calculated by simulating a high order circuit model including the relevant parasitic elements. The resulting DM emission levels are given as example in figure 2. There, the blue line describes the simulated emission level measured by the LISN, the black curve represents the worst case maximum values inclusive safety margin and the red und the green line the limits.

With the DM noise and the regulations on conducted RF emissions for the intended application (CISPR 11) the required attenuation of the DM filter could be calculated by selecting the largest peak value within the relevant range (150kHz-30MHz) and comparing this value the limits. The required filter attenuation is used to choose an appropriate DM filter topology [9] and the number of connected filter stages in series. On the basis of the filter topology the corner frequency of the filter is calculated, so that the attenuation is equal to the required one plus 6dB margin at the given frequency. With the corner frequency of the filter the $L \cdot C$ products are given. The filter damping is - among other things - determined by an upper limit for the output impedance of the filter. This limit is given by the control loop of the PFC

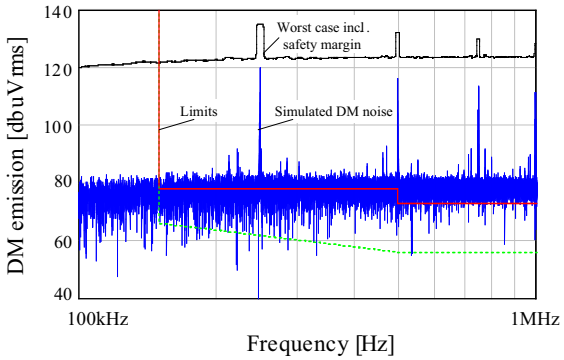

Figure 2: Simulated emission levels of DM noise, worst case values inclusive 6dB safety margin and limit values.

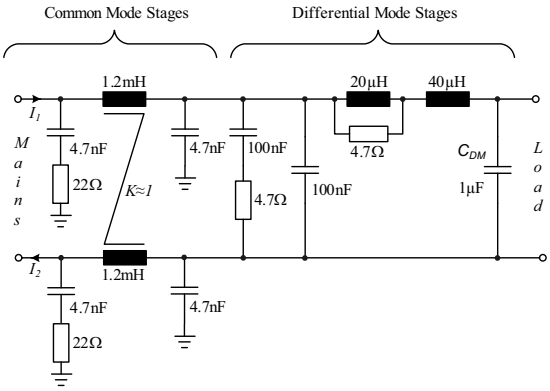

Figure 3: Circuit diagram of the discrete EMI-Filter

converter, since the output impedance influences the stability of the system.

Now, the filter topology for the DM, the corner frequencies and the required damping are known. Depending on the number of filter stages and the topology there are some degrees of freedom for the choice of the component values. These degrees of freedom are used to minimise the overall volume of the DM EMI-filter.

As with DM noise, the required attenuation for the CM could be calculated from CM noise simulation and given limits. With the required attenuation the filter topology is selected and the corner frequency of the filter is calculated. Since the Y-capacitors size is limited by the regulations - the current to ground must not exceed 3mA at 50Hz - the value of the inductance is determined for Y-capacitors values close to the maximum allowed ones according to electrical safety regulations. In order to damp the CM filter properly some resistors in series with the capacitors are added.

The resulting filter topology and the component values are shown in figure 3. For the common mode choke Vitroperm^{TM} from Vacuumschmelze has been chosen in order to minimise the inductor volume. The measured insertion loss of the discrete filter is given in figure 4 and the design of the filter is shown in figure 5 and the overall volume is 47.4cm^3 (48mm×38mm×26mm). In

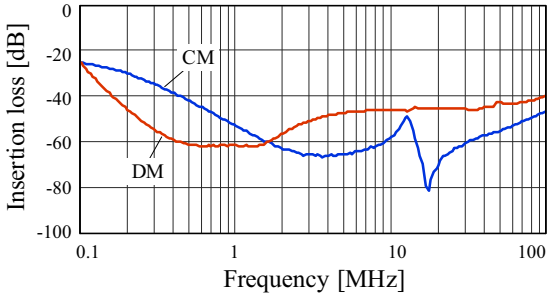

Figure 4: Insertion loss of the discrete EMI-Filter

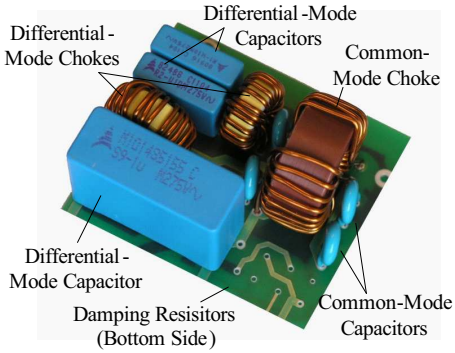

Figure 5: Photo of the discrete EMI-Filter

the next step integrated filters with comparable performance are designed.

III. Passive Hybrid EMI filters

In order to reduce the filter volume and simplify the manufacturing the discrete EMI filter components are - if possible - integrated into a PCB, which could be manufactured with state-of-the-art PCB process technology. The circuit diagram of the passive hybrid integrated EMI filter is shown in fig. 6(a) and the filter parameters are given in table II.

In comparison to the discrete filter the DM inductors are arranged symmetrically in the lines and the DM inductance value is slightly larger. This results in smaller CM capacitors (100nF / 800nF instead of 100nF / 1μF) for the same corner frequency of the DM filter.

The assembly of the passive hybrid filter is shown in figure 6(b). Each of the coupled DM inductors is integrated by four 105μm copper layers, which are connected in parallel in order to minimise the ohmic losses. The copper layers are covered on both sides by a 1.25mm thick layer of FPC 351 (Epcos). Each coil consists of 17 turns, which are arranged at the edge of the 80mm×80mm PCB. The total width of the coils is 20mm. Thus, there is a 40mm by 40mm large region in the centre of the board where the winding of the CM choke could be integrated as shown in figure 6(b). Due to the large CM inductance a planar ELP 32 core is used for the CM inductor. The DM coils use two FPC and one μ-Metal (VAC) layer as magnetic path.

The damping of the passive integrated filter mainly results from the frequency dependent resistors $R(f)$ which represent the high frequency losses of the coils due to skin- and proximity effect. The geometry of the coils is designed so that the DC losses are low but the high frequency losses are high enough to damp the filter. The damping elements at the input and output of the filter remain in order to attenuate oscillations caused by the line or the input impedance of the converter. The capacitors and the resistors of the damping elements could also be integrated in the PCB using dielectric and resistive layers (e.g. HiK^{TM}-material and OHMEGA-PLY / Carbon Paste respectively). In order to simplify the testing of the filter the capacitors and resistors of

Table II: Parameters of the passive hybrid EMI filter

Parameter	Value
DM Inductance	182 μH
Number of turns	17
Coupling factor	0.86
Loss in DM choke	17.8 W
CM Inductance	1.5 mH
Number of turns	16
Loss in CM choke	8.4W
Size [mm]	80×80×7.2
Boxed volume	46.1 cm^3

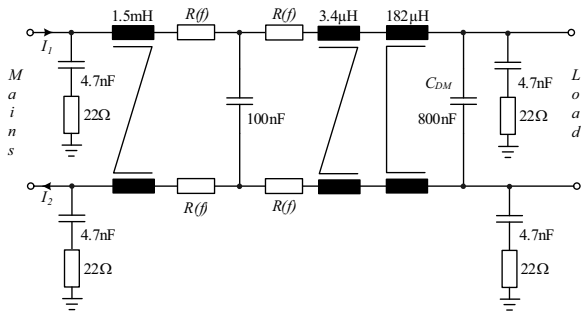

(a) Circuit diagram of passive integrated

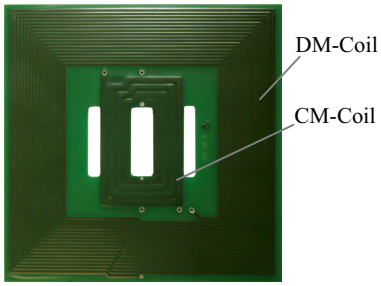

(b) 4-layer PCB for 1 DM Coil / $^1/_2$ CM-Coil

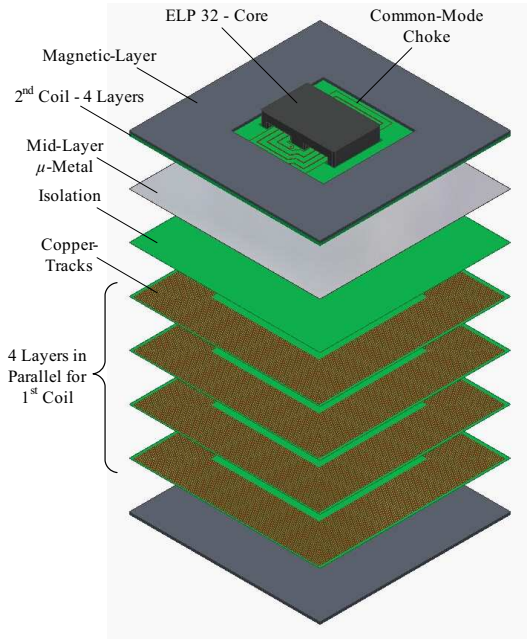

(c) Layer stack of passive integrated filter

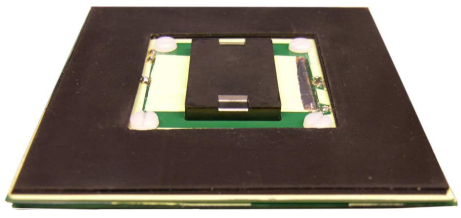

(d) Photo of assembled passive filter

Figure 6: Circuit diagram (a), photo of PCB (two are need for the passive filter) (b), layer stack (c) and photo of assembled passive hybrid filter (d).

the damping network are realised by SMD components in the prototype.

A. Design of Coupled Inductors

The symmetrically arranged DM inductors are implemented by two coupled inductors. In figure 7 the principle of operation is shown for DM (a) and CM (b) excitation is shown (PCB cross section with two parallel layers each).

The assembly of the coupled coils consists of the following five different layers:

- Magnetic layer at the top (e.g. Mag-Lam, FPC, μ-Metal) - thickness: $\sim$ 1mm
- Winding of coil 1 consisting of one or more copper layers connected in series and/or parallel
- Thin layer ($\sim$100 μm) of magnetically and electrically conductive μ-Metal^{TM} (comparable to silicon steel)
- Winding of coil 2 (usually same design as coil 1 but reverse winding direction)
- Magnetic layer at the bottom (same as at the top)

In figure 7(a) the current and the flux direction in the coils for differential mode excitation is shown. The current I_1 in the upper coil causes the magnetic flux Φ_{DM1} and the current I_2 in the lower coil Φ_{DM2}. In the μ-metal layer in the middle both DM fluxes cancel each other (dashed lines) so that there is no flux in the μ-metal layer for a symmetric design under DM excitation. Consequently, the value of the DM inductance of the integrated coils is independent of the size of the μ-metal layer.

In figure 7(b) the current direction and flux distribution for CM excitation is given. Due to symmetry reasons the common mode flux of both coils Φ_{CM1} and Φ_{CM2} adds up and flows in the middle between the two coils through the gap and the μ-Metal layer. The shorter the gap is the lower is the magnetic reluctance of the path and the higher is the CM inductance.

The ratio between DM and the CM inductance values defines the coupling between the two coils (the larger L_{CM}/L_{DM} the lower is the coupling). This relation is controlled by the horizontal extension of the μ-metal layer. If this layer starts at the very left side and ends at the very right side of the coil the coupling is approximately zero. In figure 8 the dependence of the coupling factor k on the length of the μ-Metal layer is shown for a test assembly. These results habe been obtained by the developed design procedure (described later) and are validated by measuring the coupling coefficient for different extensions of the μ-metal layer.

Since the CM current / flux has almost no spectral components below the switching frequency the amplitude of the CM flux is small. Therefore, the μ-Metal layer, which has a saturation flux density of approximately 0.8T, could be very thin ($\approx$100μm).

In [12] the distributed capacitance between a winding and a conductive layer is transformed into a network consisting of three capacitors (cf. fig. 9). The capacitance C is the static capacitance between the winding and the conductive layer (cf. [13]). As the equivalent capacitance parallel to the winding is negative it could be used to cancel the parasitic capacitance C_P of the winding (cf. [8] and [4]). Thus, the distributed capacitance caused by the μ-Metal layer could be used to reduce the value of the capacitance

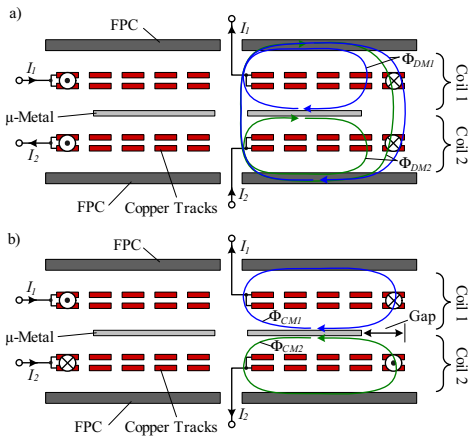

Figure 7: (a) Diagram of coupled coils (b) design of the coils.

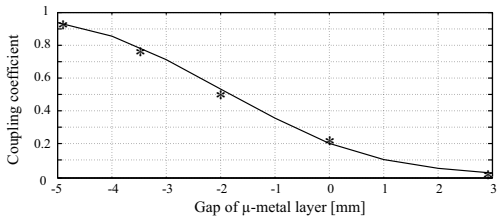

Figure 8: Dependence of the coupling factor k on the length of the μ-Metal layer (cf. figure 7) - measured values at *.

in parallel to the winding and to increase the frequency of the first resonance of the coil if the layer is connected to ground. The value of the static interlayer capacitance C is calculated within the design procedure and adjusted by varying the vertical distance between the μ-Metal layer and the winding.

With the construction shown in figure 7, where the CM flux flows through the μ-metal layer in the middle, the DM inductance is larger than or equal to the CM inductance due to the coupling of the DM flux. If a larger CM inductance and a lower DM inductance is needed, the winding direction of one coil has to be changed. In this case a thicker magnetic middle layer (twice the thickness of the outer magnetic layer) is needed, because the relatively large DM flux flows through the middle layer. The achievable maximum values for the CM and the DM inductances are the same for both design possibilities, if the distance between two magnetic layers above and below one PCB (i.e. the gap) is the same. Consequently, the design with the changed winding direction leads to an increased volume and larger magnetic losses for the same maximum achievable inductance values and should only be used in case a CM inductance is needed, which is larger than the DM one.

B. Design Procedure

The integrated inductors of the EMI-filter are designed using an automated design procedure, whose flow chart is given in figure 10. This procedure, which is based on finite element simulations (COMSOL^{TM}) and analytic calculations, will be shortly explained in the following.

At the beginning of the procedure different parameters like the number of layers in the PCB N_L, the number of parallel connected layers N_{LP}, PCB size B×T, the vertical distance between the layers t_ν, etc. must be specified by the user. These parameters are not varied within the design procedure since they mainly depend on requirements not related to the filter itself. On the other hand, there are parameters like the number of turns N, the PCB width w_{Track} and distance w_{Track}, the thickness t_C of the magnetic layers, etc. which could be varied in order to optimise the design.

With the parameters given in MATLAB^{TM} input-files for FEM simulations describing the geometry and boundary conditions are automatically generated by the programme. In the next step FEM simulations are carried out by the programme for different setups (CM- and DM excitation, different voltage distributions)- cf. figure 11. On the basis of the magnetic and electric energies the inductance and capacitance values are calculated. Furthermore, the magnetic field distribution is used to calculate the HF resistances of the coils analytically. Thereafter, the

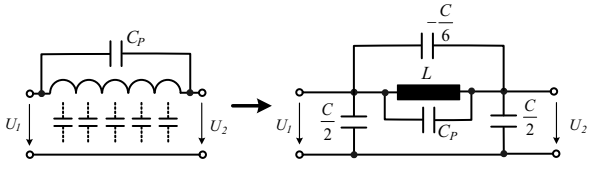

Figure 9: Equivalent network for a distributed capacitance between a winding and a conductive layer according to [12]

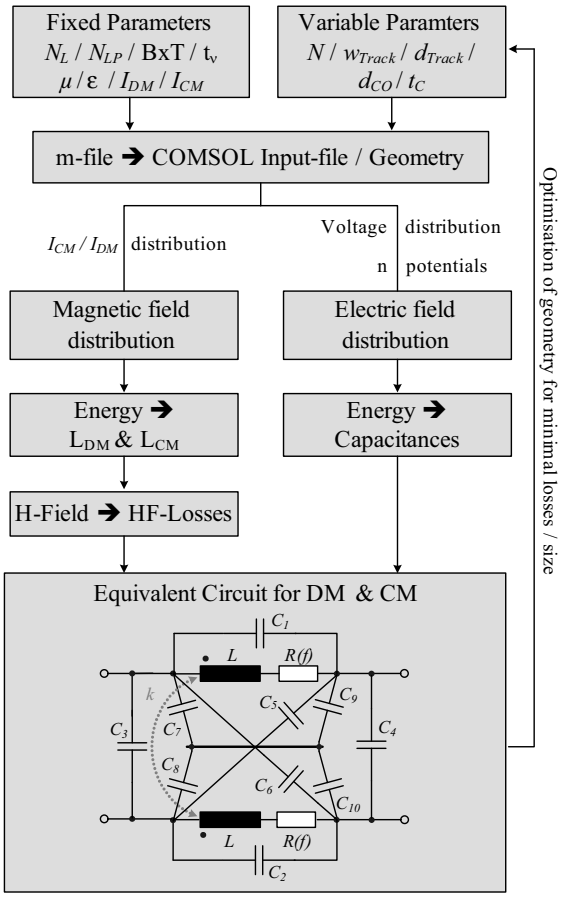

Figure 10: Flowchart of the design procedure for the integrated coils.

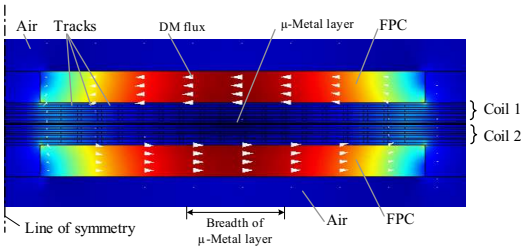

Figure 11: DM-Finite element simulation of passive hybrid integrated EMI filter.

calculated values are transformed into equivalent circuit values of the EMI filter.

The described design routine offers the possibility to be used within an optimisation routine, which varies for example the number of turns and the design of the tracks in order to minimise the filter volume or to maximise the efficiency.

IV. Active Hybrid EMI Filter

The discrete and also the passive hybrid EMI filter require a large common mode inductance because the value of the Y-capacitance is limited by regulations and because the corner frequency of the filter must be low due to the CM emission level. Since the amplitude ratio of the high frequency CM current and the DM current at the line frequency is usually relatively small, the volume of the CM inductor could be reduced by using an active filter. This active EMI filter consists of two small common mode inductors, two 20nF capacitors, a measurement network and an analog amplifier as shown in figure 12(a) (cf. [14]).

With the measurement network the CM voltage V_{CM} caused by the converter/load is measured via the two 1nF capacitors. The CM voltage is amplified by an analog Class-A amplifier, which injects an inverted CM current via the two 22nF capacitors into the filter network. Thus, the CM current resulting from the load

Table III: Materials for Capacitance Integration

	C-Lam	HiK	Rogers
Permittity	11		10.2
Breakdown Voltage	30kV/mm	1kV	-
$\tan\delta$	0.02	0.02	0.0027
Capacitance per cm^2	0.2nF	0.2nF	0.2nF

is cancelled/reduced by the active filter. Due to the limited gain of the amplifier and non-ideal components the amplitude of the CM voltage/current is only reduced by approximately 20dB in best case.

Moreover, the limited bandwidth of the amplifier requires a reduction of the gain at higher frequencies in order to guarantee the stability of the system. This also results in a decline of the CM voltage/current cancellation at higher frequencies. In the limited frequency range from approximately 100 kHz up to 6 MHz, where the voltage/current cancellation is working, the effective CM capacitance is increased very much by the amplifier. Thus, a smaller CM inductance can be used to obtain the same corner frequency / attenuation as for the CM filter of the discrete/passive hybrid filter.

The decline of the attenuation due to the limited amplifier bandwidth is not critical, because also the effective impedance of a large common mode choke decreases with increasing frequency due to the parasitic capacitance which causes a parallel resonant behaviour of the choke at higher frequencies.

The two common mode inductors needed for the active EMI filter are integrated in the PCB as described in the previous section. The final design of the complete active hybrid integrated filter is shown in figure 12(b). There, the components of the

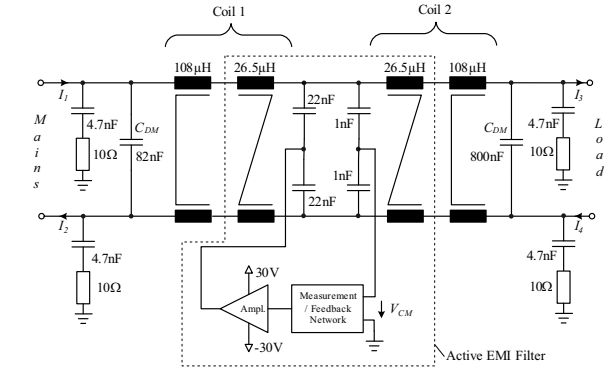

(a) Circuit Diagram of active hybrid

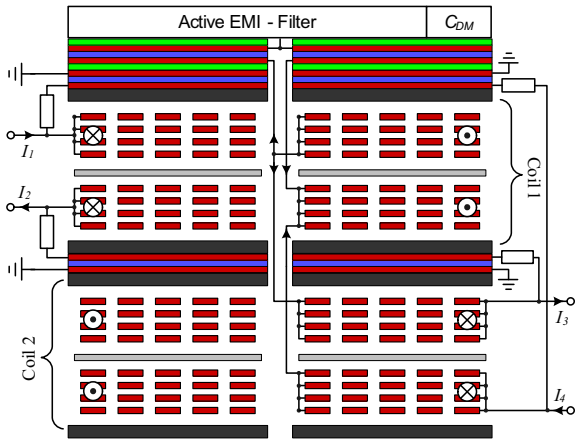

(b) Construction of active hybrid filter

Figure 12: (a) Circuit diagram of the active hybrid integrated EMI-filter (b) Design of the active hybrid integrated EMI-filter.

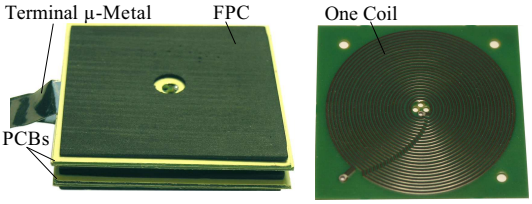

(a) Picture of active filter *(b)* PCB of one layer

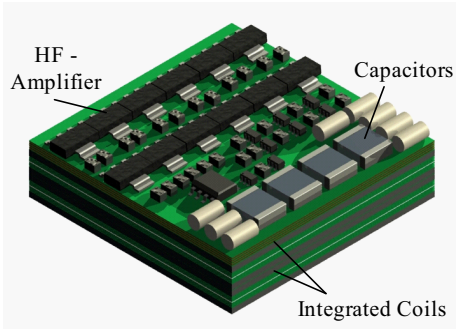

(c) 3D drawing of final assembly of active filter

Figure 13: (a) Picture of assembled active hybrid EMI filter (b) Picture of the PCB of one layer.

Table IV: Parameter of Active Hybrid EMI-filter

Parameter	**Value**
DM Inductance	216 μH
CM Inductance	53 μH
Losses	28.4 W
Size [mm]	60×60×16.2
Volume	27.3 cm^3

active filter are mounted on top of the PCB. Below the active filter the capacitances for measuring the CM voltage and injecting the CM current as well as the relatively small capacitances for damping resonances at the input and the output of the filter can be integrated. Due to the planar design these capacitors show low ESR and ESL. In table III some dielectric materials for integrating capacitances into PCBs are shown.

Due to the relatively low permittivity of these materials the large capacitors for the differential mode C_{DM} still have to be realised as SMD capacitors which are mounted on top of the PCB besides the active filter components.

In figure 13(a) the examined prototype of the coupled coils for the active filter is shown. It consists of four layers of FPC 302 from Epcos with a thickness of approximately 1.3mm, four PCBs each with four 105μm layers of copper for the coils (cf. fig. 13(b)) and two layers of μ-metal. At the left hand side the terminals of the μ-metal layers are shown with which the layers could be connected to ground in order to reduce the parasitic capacitance. Below the pictures a 3D drawing of the final assembly of the integrated active hybrid filter is shown in figure 13(c). In table IV the technical parameters of the active EMI-filter are listed.

V. Comparison of the EMI-filters

In order to compare the performance of the different filters measured transfer functions, losses and volume of the discrete, the passive and the active hybrid filter are presented in the following.

Usually, insertion loss measurements, i.e. the ratio U_2/U_{Noise}, are used to characterise EMI filters. However, these measurements also include the attenuation which results from the source impedance of the measurement circuit (usually 50Ω) and the filter capacitors (cf. fig. 14). The source / internal impedance of

Table V: Calculated and measured parameters of the three compared EMI-filters

Parameter	Discrete Filter	Passive Filter			Active Filter		
		calculated	measured	modified	calculated	measured	modified
DM Inductance	60 μH	194 μH	182 μH	206 μH	132 μH	108 μH	150 μH
CM Inductance	1.2 mH	1.45 mH	1.5 mH	1.45 mH	65 μH	53 μH	73 μH
Losses @ 7.7A$_p$	3.56 W	2x(7.6+3.7)W	2x(8.9+4.2)W	2x(2.2+3.7)W	4x5.7W+6W	4x7.1W+6.1W	4x1.6W+6W
Efficiency @110V	99.4 %	96.2 %	95.6 %	98 %	95.2 %	94.3 %	98 %
Efficiency @230V	99.8 %	99.1 %	99.0 %	99.5 %	98.1 %	97.9 %	98.8 %
Total Volume	47.4 cm^3	-	36.1 cm^3	27.4 cm^3	-	27.3 cm^3	21.3 cm^3

the noise source and with that also the additional attenuation depend very much on the converter topology and the design of the converter. In order to obtain information about the filter attenuation which is independent of the source impedance, the transfer function, i.e. the ratio U_2/U_1, is used in the following. The input voltage of the filter U_1 for a given source impedance could be calculated with the input impedance Z_{IN} of the EMI filter, which is also presented in the following. The additional attenuation because of the source impedance could be seen in figure 15, where the DM insertion loss and the transfer function for the active filter are plotted in the same graph.

In figure 16 the CM and the DM attenuation and the input impedance of the passive hybrid filter is given. There, the two curves for the CM show the different attenuation of the filter when the μ-metal layer is connected to ground or free floating. Due to the additional parasitic capacitances (cf. fig 9) the HF behaviour of the filter is improved. The resonant peak of the CM attenuation between 400kHz and 500kHz results from the characteristic frequency of the CM choke.

Due to the large source impedance of the PFC converter (boost inductor: 187μH - cf. fig. 1) the DM attenuation of the passive filter increases very much in the frequency range from 100kHz to 1MHz, since the input impedance of the filter is relatively low in this region. For example, at 100kHz approximately additional 20dB result from the large source impedance resulting in an effective attenuation larger than 40dB for DM at 100kHz.

In the considered frequency range, the input impedance of the active filter for DM is even lower than the one of the passive filter, what leads to a larger additional damping due to the source impedance (cf. fig. 17). Consequently, the DM attenuation of the two integrated filters is comparable to the one of the discrete

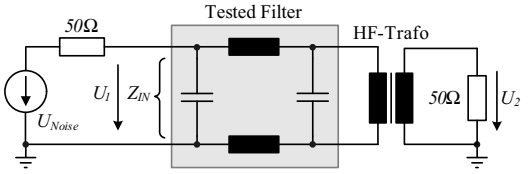

Figure 14: Circuit for the measurement of the transfer (U_2/U_1) function (filter attenuation) and the input impedance.

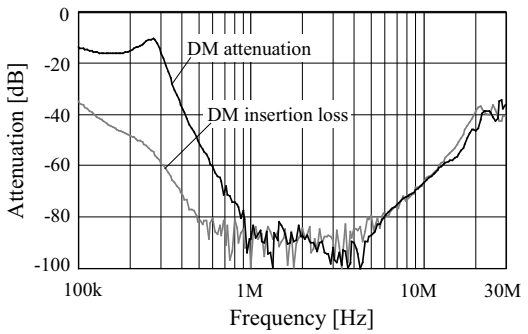

Figure 15: Comparison between the DM attenuation / transfer function (U_2/U_1) and insertion loss of the active hybrid filter.

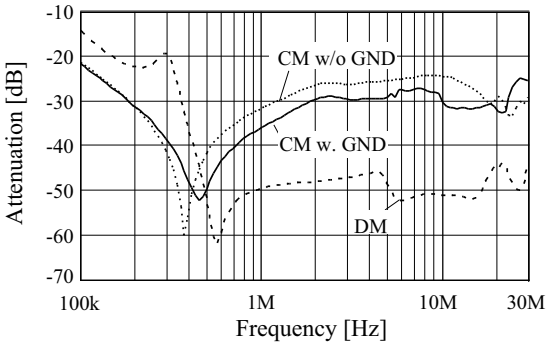

(a) Transfer function of active filter

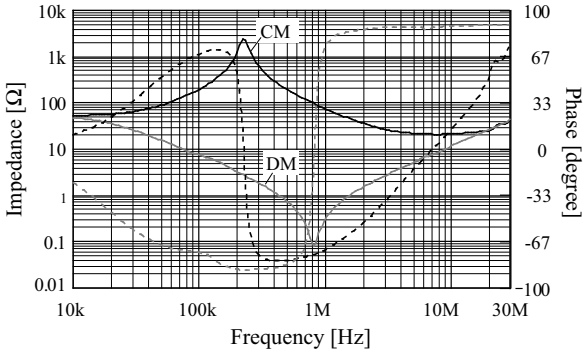

(b) Input impedance in CM & DM

Figure 16: (a) Transfer function of the passive filter for CM with (w. GND) and without connection of the μ-metal layer to ground (w/o GND) and for DM. (b) Input impedance of the filter at the load side for CM and for DM with phase (dashed lines).

filter and even exceeds it a bit.

The comparatively low resonance frequency of the CM choke of the passive integrated filter results in a CM attenuation curve which is not as good as the one of the discrete filter. The reason for this are the parasitic capacitances resulting from the planar winding design. A new design of the CM choke, which leads to reduced parasitic capacitances and also lower losses, is shown in figure 18. There, the core is integrated in the PCB by magnetic layers and the winding consists of wire or in case of low power applications of PCB tracks. This design will be evaluated and the results presented in a future paper.

In figure 17(a) the CM attenuation of the active integrated filter is shown. There, it could be seen that the amplifier results in an additional attenuation of 15-20dB in the frequency range from 400kHz to 4MHz. The resonant peak at approximately 160kHz is caused by the limited gain of the amplifier. As simulations show the gain could be increased by using transistors with a higher transition frequency in the power stage of the amplifier. The improved behaviour will also presented in a future publication.

The resonant peak around 2MHz in the CM attenuation of the active integrated filter is caused by the characteristic frequency of the integrated coils.

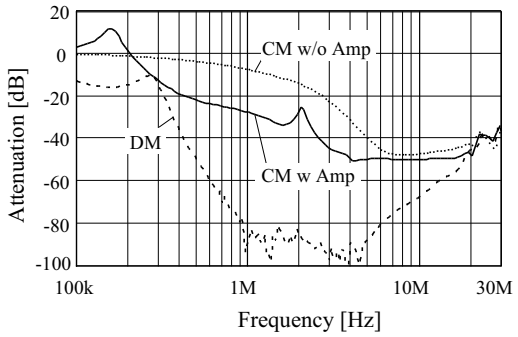

(a) Transfer function of active filter

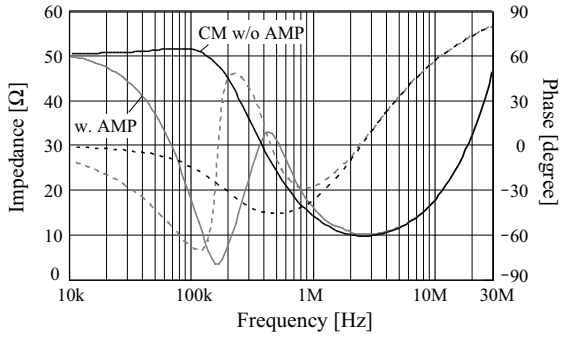

(b) Input impedance in CM

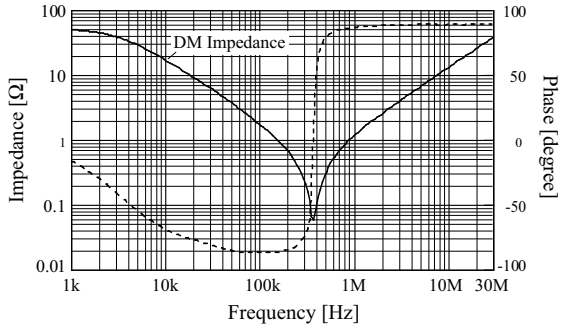

(c) Input impedance in DM

Figure 17: (a) Transfer function of the active filter for CM with (w. AMP) and without Amplifier (w/o AMP) and for DM. (b) Input impedance of the filter at the load side for CM with (w. AMP) and without Amplifier (w/o AMP) with phase (dashed lines) (c) Input impedance of the filter at the load side for DM with phase (dashed lines).

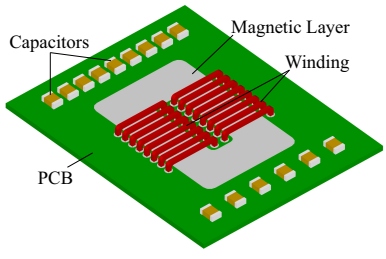

Figure 18: New design of the CM choke.

In table V the volume, the losses and the efficiency of the three EMI filters are given. The values in the "modified" columns result from using Vacoflux 48 (VAC), which has a saturation flux density of 2T, instead of FPC 351/302 as magnetic layer. As can be seen the losses and the volume of the integrated filters can be reduced very much so that the efficiency of the integrated filters is comparable to the one of the discrete filter but the volume is reduced by almost 50%.

VI. Conclusion

The EMI filter is a significant part of a converter in terms of size and cost. Thus, the size of EMI filters must be reduced and the manufacturing simplified in order to increase the power density and to reduce the cost of converter systems.

In the paper a design procedure and measurement results for two different integration approaches - a passive hybrid integration in a PCB and an active hybrid integration with an active EMI filter - are presented. The filter are integrated into a PCB board which could be manufactured with standard PCB manufacturing technology. Due to the integration the filter volume is reduced up to 40% while maintaining a high efficiency.

References

[1] J.T. Strydom, "*Electromagnetic Design of Integrated Resonator-Transformers*," Ph.D. Thesis, Rand Afrikaans University, South Africa, 2001.

[2] J.D. van Wyk, F.C. Lee, Z Liang, R. Chen, S. Wang and B. Lu, " *Integrating Active, Passive and EMI-Filter Functions in Power Electronic System: A Case Study of Some Technologies*," Power Electronics, IEEE Transactions on, Volume 20, Issue 3, May 2005, Page(s):523 - 536.

[3] E. Waffenschmidt, B. Ackermann and J.A, Ferreira, "*Design method and material technologies for passives in printed circuit Board Embedded circuits*," Power Electronics, IEEE Transactions on Volume 20, Issue 3, May 2005, Page(s):576 - 584.

[4] R. Chen, J.D. van Wyk, S. Wang and W. G. Odendaal, "*Improving the Characteristics of Integrated EMI Filters by Embedded Conductive Layers*," Power Electronics, IEEE Transactions on, Volume 20, Issue 3, May 2005, Page(s):611 - 619.

[5] T. Farkas and M.F. Schlecht, "*Viability of Active EMI Filters for Utility Applications*," Power Electronics, IEEE Transactions on, Volume 9, Issue 3, May 1994, Page(s):328 - 337.

[6] L. Lawhite and M.F. Schlecht, "*Design of Active Ripple Filters for Power Circuits Operating in the 1-10MHz Range*," Power Electronics, IEEE Transactions on, Volume 3, Issue 3, July 1988, Page(s):310 - 317.

[7] T.C. Neugebauer and D. J. Perrault, "*Filters With Inductance Cancellation Using Printed Circuit Board Transformers*," Power Electronics, IEEE Transactions on, Volume 19, Issue 3, May 2004, Page(s):591 - 602.

[8] T.C. Neugebauer and D. J. Perrault, "*Parasitic Capacitance Cancellation in Filter Inductors*," 35^{th} IEEE Power Electronics Specialists Conference, PESC'04, Aachen, Germany, June 2004, Page(s):3102 - 3107.

[9] M.J. Nave, "*A Novel Differential Mode Rejection Network for Conducted Emissions Diagnostics*," IEEE 1989 National Symposium on Electromagnetic Compatibility, Denver, USA, 23-25 May, 1989, Page(s):223-227.

[10] M.L. Heldwein, T. Nussbaumer, F. Beck, J.W. Kolar, "*Novel Three-Phase CM/DM Conducted Emissions Separator*," Proceedings of the 20th Annual IEEE Applied Power Electronics Conference and Exposition, Austin (Texas), USA, March 6 - 10, Vol. 2, 2005, Page(s):797 - 802.

[11] T. Nussbaumer, M.L. Heldwein, J.W. Kolar, "*Differential Mode EMC Input Filter Design for a Three-Phase Buck-Type Unity Power Factor PWM Rectifier*," Proceedings of the 4th International Power Electronics and Motion Control Conference, Xian, China, Aug. 14 - 16, Vol. 3, 2004, Page(s):1521 - 1526.

[12] L. Oestergaard, "*Modelling and Simulation of the Diode Split Transformer*," Dissertation, Faculty of Engineering and Science at Aalborg University, 1999, Page(s):139 - 169.

[13] J. Biela, J.W. Kolar, "*Using Transformer Parasitics for Resonant Converters - A Review of the Calculation of the Stray Capacitance of Transformers*," Conference Record of the 2005 IEEE Industry Applications Conference 40th IAS Annual Meeting, Hong Kong, China, Oct. 2 - 6.

[14] M. L. Heldwein, H. Ertl, J. Biela and J. W. Kolar, "*Implementation of a Transformer-Less Common Mode Active Filter for Off-line Converter Systems*," Proceedings of the 21th Annual IEEE Applied Power Electronics Conference and Exposition (APEC), Dallas (Texas), USA, March 19-23, 2006.